AIP | Review of Scientific Instruments

A large volume cell for in situ neutron diffraction studies of hydrothermal crystallizations

Fang Xia, Gujie Qian, Joël Brugger, Andrew Studer, Scott Olsen, and Allan Pring

Citation: Review of Scientific Instruments **81**, 105107 (2010); doi: 10.1063/1.3484281
View online: http://dx.doi.org/10.1063/1.3484281
View Table of Contents: http://scitation.aip.org/content/aip/journal/rsi/81/10?ver=pdfcov
Published by the AIP Publishing

A large volume cell for *in situ* neutron diffraction studies of hydrothermal crystallizations

Fang Xia,[1,2,a] Gujie Qian,[1,3] Joël Brugger,[1,2] Andrew Studer,[4] Scott Olsen,[4] and Allan Pring[1,2]
[1]*Department of Mineralogy, South Australian Museum, North Terrace, Adelaide, South Australia 5000, Australia*
[2]*School of Earth and Environmental Sciences, University of Adelaide, North Terrace, Adelaide, South Australia 5005, Australia*
[3]*Ian Wark Research Institute, University of South Australia, Mawson Lakes Campus, Mawson Lakes, South Australia 5095, Australia*
[4]*The Bragg Institute, Australian Nuclear Science and Technology Organisation, Locked Bag 2001, Kirrawee DC, New South Wales 2232, Australia*

(Received 21 May 2010; accepted 9 August 2010; published online 19 October 2010)

A hydrothermal cell with 320 ml internal volume has been designed and constructed for *in situ* neutron diffraction studies of hydrothermal crystallizations. The cell design adopts a dumbbell configuration assembled with standard commercial stainless steel components and a zero-scattering Ti–Zr alloy sample compartment. The fluid movement and heat transfer are simply driven by natural convection due to the natural temperature gradient along the fluid path, so that the temperature at the sample compartment can be stably sustained by heating the fluid in the bottom fluid reservoir. The cell can operate at temperatures up to 300 °C and pressures up to 90 bars and is suitable for studying reactions requiring a large volume of hydrothermal fluid to damp out the negative effect from the change of fluid composition during the course of the reactions. The capability of the cell was demonstrated by a hydrothermal phase transformation investigation from leucite ($KAlSi_2O_6$) to analcime ($NaAlSi_2O_6 \cdot H_2O$) at 210 °C on the high intensity powder diffractometer Wombat in ANSTO. The kinetics of the transformation has been resolved by collecting diffraction patterns every 10 min followed by *Rietveld* quantitative phase analysis. The classical *Avrami/Arrhenius* analysis gives an activation energy of 82.3 ± 1.1 kJ mol^{-1}. Estimations of the reaction rate under natural environments by extrapolations agree well with petrological observations. © *2010 American Institute of Physics.* [doi:10.1063/1.3484281]

I. INTRODUCTION

Hydrothermal crystallizations are complex reactions involving molecular level nucleation and crystal growth, and nano- to macrolength scales of fluid transport of aqueous species.[1] Typical examples are pseudomorphic mineral replacement reactions which are common features in rocks,[2] and can feature some coupling between the dissolution of the parent mineral and the crystallization of the new phase, and in some cases can result in nanometer-scale pseudomorphic replacement of the parent minerals.[3] These reactions are responsible for the formation of minerals and mineral assemblages under natural hydrothermal environments as well as industrial-scale chemical production.[4,5] A thorough understanding of the mechanisms and kinetics of these reactions has significant theoretical and practical implications but usually requires combined information from *ex situ* characterization of the reaction products and *in situ* dynamic observation of the reaction progress. Most previous studies were, however, only based on *ex situ* characterization due to the lack of systems for *in situ* experiments, and thus clearer understanding of hydrothermal crystallization awaits complementary *in situ* information.

In this context, considerable effort has been devoted to the development of *in situ* powder diffraction systems for hydrothermal experiments because powder diffraction is the ideal technique for the detection and quantification of phase evolution during crystallization. In view of the high fluxes achieved by modern synchrotron x-ray and neutron beams, the biggest challenge for *in situ* studies is the scarcity of suitable hydrothermal cells that can fit within modern synchrotron x-ray or neutron diffraction beamlines, while operating at elevated temperatures and pressures. For this reason, several hydrothermal cells have been developed in the past two decades. For examples, Polak *et al.*[6] (1990) developed a 4 ml cell at Birkbeck College (U.K.) for neutron diffraction (ND) studies of tobermorite and zeolite syntheses. Later, Evans and co-workers[7,8] (1995) constructed a 25 ml cell at Oxford University (U.K.) and successfully used it in the study of microporous materials syntheses by synchrotron energy dispersive x-ray diffraction. Norby *et al.*[9,10] (1997 and 1998) developed two ca. 2 μl capillary cells at Brookhaven National Laboratory (USA) for angle dispersive x-ray powder diffraction (ADXRD), and employed them in hydrothermal zeolite crystallizations. After that, Walton and

[a]Author to whom correspondence should be addressed. Electronic mail: fang.xia@adelaide.edu.au.

co-workers[11,12] (1999) designed a 23 ml cell at Oxford University (U.K.) for ND studies of hydrothermal syntheses of various inorganic materials. O'Neill *et al.*[13] (2006) developed a 280 ml mechanical pump-driven flow-through cell at University of Adelaide (Australia) for ND study of sulfide alteration. Very recently, Webster *et al.*[14] (2009) designed a 0.1 ml flow cell at CSIRO (Australia) for ADXRD investigation of scale formation under Bayer processing conditions.

These cells have contributed to the understanding of hydrothermal reactions, but their applications are limited to certain circumstances because they suffer problems such as small fluid volume, high beam absorbing/scattering by the cell body, and more importantly, low operation temperatures and pressures. Many emerging investigations of hydrothermal crystallizations require higher temperature and pressure and larger fluid volumes, and hence demand new cells to carry out *in situ* experiments. The large volume is essential to keep the fluid composition relatively constant so that the mechanism and kinetics can be studied under tightly constrained solution chemistry.[15] This simplifies the data interpretation because hydrothermal reactions are usually complex and a significant change of fluid composition during the course of the reaction can change the mechanism drastically.[3,16,17]

To achieve a higher working temperature and pressure, and a larger fluid volume, we have previously constructed a thermosyphon driven flow-through cell and commissioned on Wombat, Australian's new high intensity powder diffractometer at the OPAL research reactor, run by Nuclear Science and Technology Organization (ANSTO).[18] The cell worked smoothly but the thermosyphon is sensitive to local temperature and air flow variations in the neutron guide hall. In practice, the temperature profile along the flow-through loop is not always stable during the course of hydrothermal reactions. For a more stable temperature profile and for more flexible sample loading, troubleshooting, and parts replacement to suit specific solution composition, a new design was required. We have further designed and constructed a 320 ml simpler static cell which is much more compact and robust to operate. This cell has been successfully commissioned on Wombat in ANSTO as well, and will be described in the following sections.

II. CELL DESIGN

The design of the cell is based on modification of laboratory closed cells (e.g., Parr autoclaves), which have excellent flexibilities in volume, chemical stability, and operation temperature and pressure.[19] These cells have been used in many laboratory hydrothermal crystallization studies, but are not suitable for *in situ* diffraction experiments because of two main drawbacks: (i) the cell volume in the beam path is too large which would lead to significantly increased background as a result of scattering by the fluid phase, and (ii) the cell body severely affects the sample signals by absorbing x-ray or neutrons, and also giving very strong diffraction peaks in the diffraction patterns that may flood detectors and/or hide peaks from the sample. Therefore, the aim of the current design was to overcome these drawbacks while still maintaining the flexibilities of laboratory cells. The outline of the new cell is shown in Fig. 1.

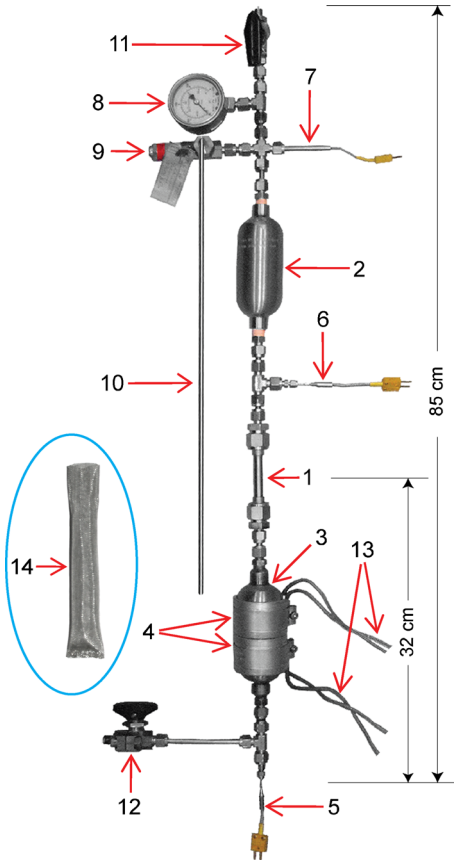

FIG. 1. (Color online) The cell. (1) Ti–Zr alloy sample compartment; (2) 150 ml expansion vessel (Swagelok®, 316 L-HDF4–150); (3) 150 ml fluid reservoir (Swagelok®, 316 L-HDF4-150); (4) two tabular heaters (Helios®, 690 W total); (5)–(7) *K*-type thermocouples, measuring the temperatures at (5) the center of the fluid reservoir, (6) the top of the sample compartment, and (7) near the pressure relief valve; (8) pressure gauge (Swagelok®, 0–10 MPa); (9) pressure relief valve (Swagelok®, 5–10 MPa, R3A-C); (10) condensation tube (Swagelok®, $\frac{1}{4}$ in. tubing); (11) top ball valve (Swagelok®, SS-4SKPS4); (12) bottom fill/drain ball valve (Swagelok®, SS-33PS4); (13) power leads of the heaters, connecting to a temperature controller (Shinko® JCR-33A-S/M); (14) enlarged view of the sample tube constructed from 316-type stainless steel mesh (Locker Group®, aperture size Φ47 μm). The components are connected by Swagelok® $\frac{1}{4}$ in. tubing, tees, and crosses, and nuts. The support system, the aluminum/polycarbonate shield, and the other ancillary components are shown in Fig. 2.

To overcome the first drawback, the cell was designed to have a dumbbell configuration. The thin sample compartment (item 1, Fig. 1) at the center can accommodate a few grams of solid sample. Two stout 150 ml cylinders above (item 2, Fig. 1) and below (item 3, Fig. 1) the sample compartment hold most of the hydrothermal fluid. The cylinders are connected to the sample compartment via sections of $\frac{1}{4}$ in. stainless steel *Swagelok*® fittings. The lower cylinder is used as the fluid reservoir and the upper one as the fluid expansion vessel at elevated temperatures. The solid sample is held in an end-sealed cylinder-shape 316-type stainless steel mesh tube (item 14, Fig. 1), which can be firmly held in the sample compartment by force of friction.

To overcome the second drawback, the sample compartment was constructed from a zero-scattering Ti–Zr alloy (67.7 at. % Ti, 32.3 at. % Zr, New Metals and Chemicals

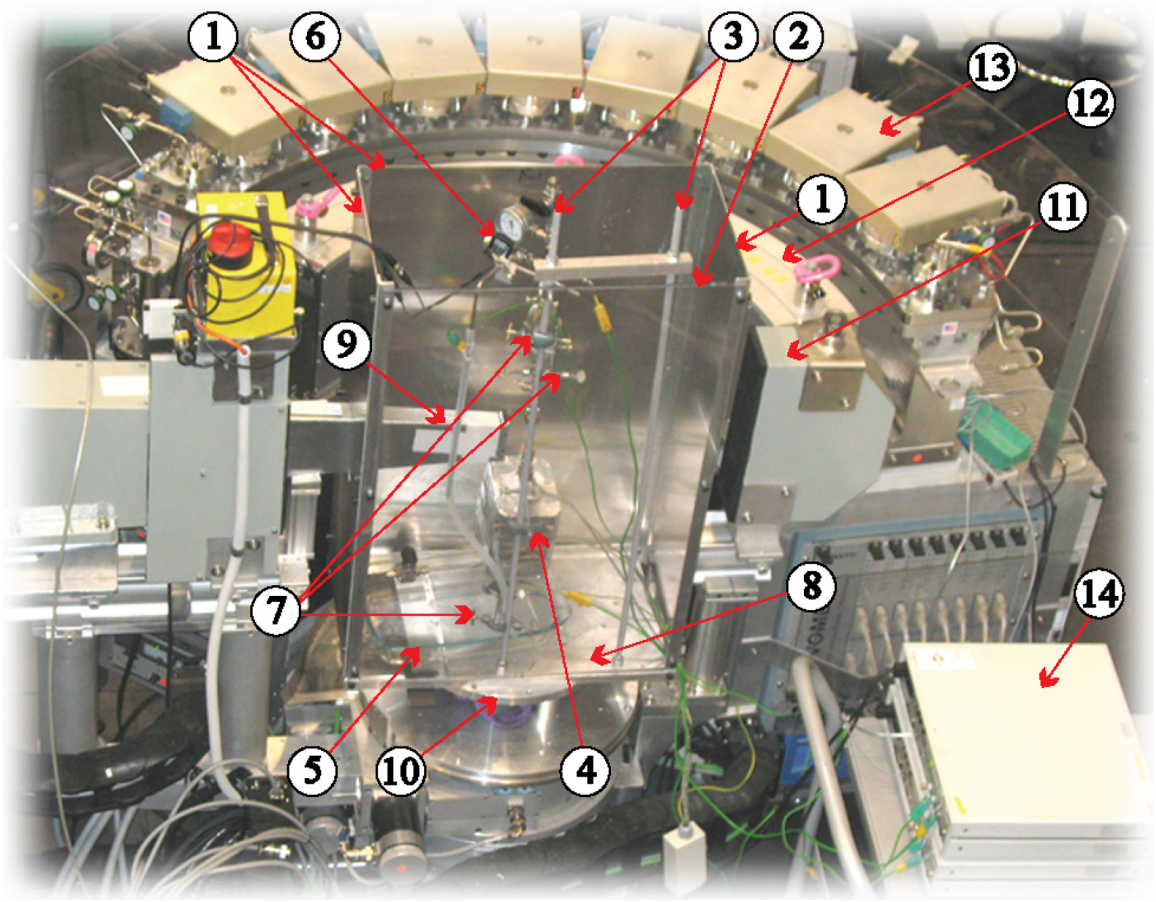

FIG. 2. (Color online) Setup of the hydrothermal cell on Wombat, the high intensity powder diffractometer in ANSTO. (1) Aluminum shield; (2) front transparent polycarbonate shield; (3) threaded support rods; (4) aluminum foil wrapped ceramic insulation block; (5) Pyrex® glass spill tray; (6) surveillance camera; (7) support clamps; (8) support base; (9) neutron beam guide; (10) sample stage; (11) neutron beam stop; (12) collimator; (13) detector; (14) temperature-recording unit (LakeShore®, Model 340).

Ltd., Waltham Abbey, U.K.), which has a zero average neutron scattering length, thereby giving no diffraction peaks in the patterns. To reduce the absorption, the Ti–Zr alloy at the beam path was thinned to a wall thickness of 0.4 mm. With this thickness the cell wall can still withstand a high pressure owing to its relatively high mechanical strength while minimizing the neutron absorption.

The hydrothermal cell utilizes natural convection for fluid movement, so as to realize mass transport and heat transfer. The fluid is heated in the fluid reservoir by two tabular heaters (item 4, Fig. 1) insulated by ceramic blocks (item 4, Fig. 2). The heated fluid becomes less dense and rises through the sample compartment to the expansion vessel. The temperature of the fluid decreases gradually while traveling up due to natural heat loss. Therefore, the fluid at the top of the cell is always denser than that at the bottom and falls due to gravity. In this way, the convection is retained and the temperature at the sample compartment can be stably sustained (steady-state condition) over the course of the reaction. For example, when the temperature in the fluid reservoir is set to 220 °C, the temperatures at the sample compartment and at the center of the expansion tank will stabilize in a few minutes at 210 and 80 °C, respectively. Fluid convection can be improved by wrapping a spiral condenser pipe onto the expansion tank when strong convection is needed.

The other features of the cell design include: (i) the temperature and pressure are monitored by *K*-type thermal couples (items 5–7, Fig. 1) and a pressure gauge (item 8, Fig. 1), respectively; (ii) the risk of pressure overshoot is controlled by a pressure relief valve (item 9, Fig. 1), which has the ability to relieve pressure overshoots automatically by releasing part of the fluid and vapor; (iii) an external gas overpressure can be applied to the system via a ball valve (item 11, Fig. 1) at the top of the system; and (iv) the fluid is filled up from the bottom via a ball valve (item 12, Fig. 1) through a soft plastic tube and a funnel utilizing the communicating vessel principle.

This simple design has excellent flexibility. All the fittings are standard commercial products (Fig. 1), so that the volume, chemical stability, and operation temperature and pressure of the cell can be adjusted by simply changing volume and construction materials of these standard components. The ratings of the components used for building the current cell allow the system to work at temperature up to 300 °C and pressure up to 90 bars.

III. INSTRUMENTAL SETUP

The cell was commissioned on Australia's new high intensity powder diffractometer Wombat in ANSTO. The setup of the cell on Wombat is shown in Fig. 2. The neutron beam

with the wavelength of $\lambda \approx 1.54$ Å was selected using a vertically focusing germanium (115) monochromator at a take-off angle of 90°.[20] The beam size was shaped by a slit system and in this study the size was 10 mm(W) × 40 mm(H) so as to completely immerse the central part of the sample compartment in the beam. After impinging on the sample, the neutrons first traveled through an oscillating radial collimator (item 12, Fig. 2). The collimator eliminates unwanted parasitic Bragg scattering, for example from the protective aluminum shield (item 1, Fig. 2). Then the diffracted neutrons were detected by a 200 mm high position sensitive area detector spanning from 15° to 135° in 2θ (item 13, Fig. 2). The distance from the sample to the front of the radial collimator was 430 mm, providing ample space for the hydrothermal cell. The zero shift and the neutron wavelength were calibrated using an alumina (Al_2O_3) standard, and the intensities of the diffraction peaks were calibrated with an empty vanadium can.

The cell was placed on a sample stage (item 10, Fig. 2) with the aid of a support system. The support system consists of two threaded rods (item 3, Fig. 2), three clamps (item 7, Fig. 2), and an aluminum metal base (item 8, Fig. 2). For safety reason, the entire cell was encased in a cuboid-shape shield (items 1 and 2, Fig. 2). The front side of the shied is made of transparent polycarbonate (item 2, Fig. 2) for easy observation of the system during operation, while the other three sides are aluminum for easy neutron penetration (item 1, Fig. 2). A *Pyrex*® glass spill tray (item 5, Fig. 2) was placed on the base for capturing fluids from the relief valve in case of a pressure overshoot situation. The thermocouples at the sample compartment and at the pressure relief valve were connected via a temperature-recording unit (item 14, Fig. 2), to a computer in the control cabin to record the temperature profile during the experiments. The thermocouple at the heating reservoir was connected via a 10 m power lead to a temperature controller (*Shinko*® JCR-33A-S/M) placed in the control cabin. A surveillance camera (item 6, Fig. 2) was installed for remote monitoring of the pressure gauge from the control cabin. After properly loading the sample and checking the shield in place, the operators withdrew from the instrument enclosure to the control cabin. Then the temperature was set to the target value by the temperature controller, the neutron beam opened, and the data collection started.

The high neutron flux allowed the collection of high quality data with adequate counting statistics in a relatively short time. This study involved fluid phases, which significantly increased the background, hence we collected diffraction data every 10 min to balance the time resolution and adequate signal to noise ratio.

IV. *IN SITU* DIFFRACTION EXPERIMENT

The capability of the cell was demonstrated by *in situ* investigation of the hydrothermal phase transformations from leucite ($KAlSi_2O_4$) to analcime ($NaAlSi_2O_6 \cdot H_2O$). This reaction is commonly observed in natural leucite crystals found in volcanic areas, where leucite crystals are often partially or completely replaced by analcime.[21] As a consequence, the product analcime crystals retain the overall shape of the parent leucite crystals, a common mineralogical phenomenon called pseudomorphism.[2] This phase transformation has been recently shown to proceed via the interface-coupled dissolution-reprecipitation replacement mechanism,[22] in which the dissolution of leucite and the precipitation of analcime are spatially and timely coupled, i.e., continued dissolution of the parent leucite makes the local fluid supersaturated with respect to analcime, causing the local precipitation of analcime almost at the same site for leucite dissolution.[22] The progressive transformation is accompanied with a sharp phase boundary moving into the leucite crystal, leaving porous analcime with the same crystallographic orientation as leucite. The length of coupling is within nanometer scale; therefore the overall shape and internal texture of leucite is preserved by analcime.[22] The mechanism can be illustrated by the following reaction equations:

The dissolution of leucite

$$KAlSi_2O_6 \rightarrow AlO_2^- + K^+ + 2SiO_{2(aq)} \quad (1)$$

followed by the local precipitation of analcime

$$2\ SiO_{2(aq)} + AlO_2^- + Na^+ + H_2O \rightarrow NaAlSi_2O_6 \cdot H_2O. \quad (2)$$

The overall transformation from leucite to analcime can be written as

$$KAlSi_2O_6 + Na^+ + H_2O \rightarrow NaAlSi_2O_6 \cdot H_2O + K^+. \quad (3)$$

In spite of this well-understood reaction mechanism, the kinetics of the transformation is yet to be determined. The kinetics may give an insight to solve an ongoing problem regarding the origin of analcime phenocryst in igneous rocks, as whether the analcime is a primary mineral forming from the magma or is a secondary mineral transformed from leucite.[21] Our previous *in situ* neutron diffraction kinetic study on this reaction was carried out at 230 °C.[18] This study is to obtain the reaction kinetics at a second temperature, so that accurate reaction activation energy can be determined and thus the reaction rate under natural environments can be estimated.

In the hydrothermal experiments, the starting leucite was natural crystals from a volcanic area near Rome, Italy. They were hand-selected, ultrasonically cleaned, crushed, and sieved. Grain sizes between 63 and 90 μm were used in this study. Analytical grade NaCl (99.5%) (Sigma-Aldrich) was used to prepare a 0.6*M* NaCl solution using heavy water (D_2O) (provided by ANSTO) as the solvent. The reaction between 1.25 g of leucite and 200 ml of NaCl solution was conducted at 210 °C.

The reaction progress was followed by *in situ* neutron diffraction patterns. The reaction extent y was calculated by a general formula

$$y = (Y_0 - Y_t)/(Y_0 - Y_e) \times 100\%, \quad (4)$$

where Y_t, Y_0, and Y_e are the mass fractions of the reactant crystals at an arbitrary reaction time t, initially ($t=0$) and at equilibrium ($t=\infty$, in this case $Y_e=0$), respectively. The mass fractions of involved phases were obtained from the *Rietveld* phase quantification method based on the diffraction data.[23]

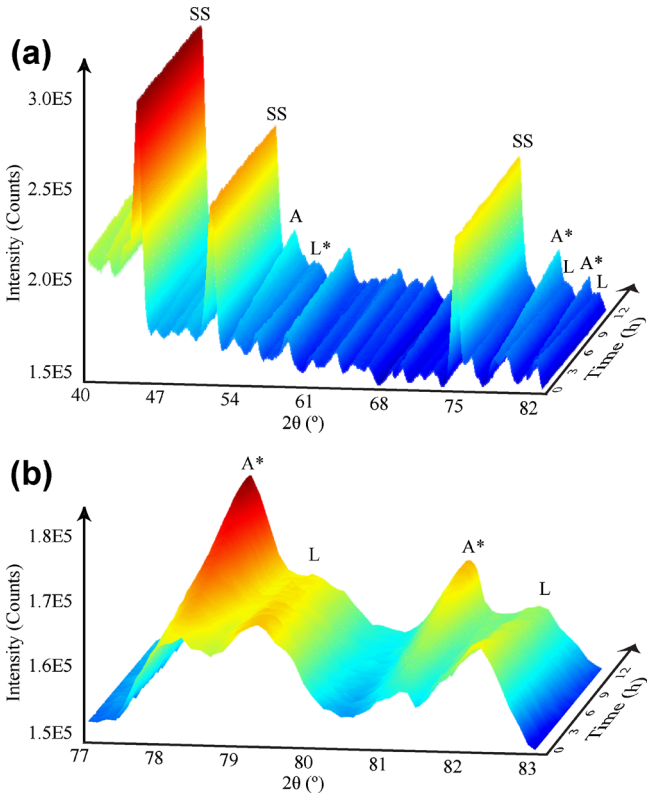

FIG. 3. (Color online) *In situ* neutron diffraction patterns of the transformation from leucite ($KAlSi_2O_6$) to analcime ($NaAlSi_2O_6 \cdot H_2O$). (a) Two-theta range from 40° to 83°, showing the progressive phase transformation; the stainless steel phase has constant peak intensities, serving as an excellent internal standard; the zero-scattering Ti–Zr alloy sample compartment has no diffraction peaks, giving an excellent flat background. (b) Two-theta range from 77° to 83°, highlighting the progressive increase of analcime peaks and decrease of leucite peaks. L=leucite peaks, A=analcime peaks, L*=overlapped peaks where leucite is the dominant phase, A*=overlapped peaks where analcime is the dominant phase, SS=stainless steel peaks.

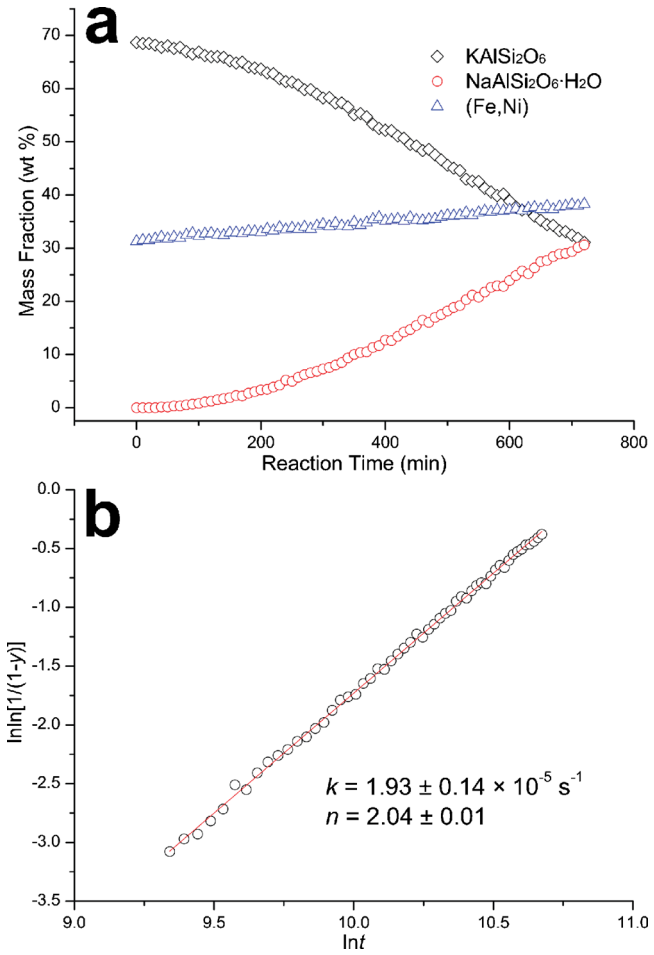

FIG. 4. (Color online) (a) Mass fractions of the three involved phases as a function of reaction time during the transformation from leucite ($KAlSi_2O_6$) to analcime ($NaAlSi_2O_6 \cdot H_2O$). Note that the total mass of the sample changed from 1.25 g at the beginning of the reaction to 0.92 g at the end because of the loss of small particles from the mesh tube; however, the mass of the stainless steel mesh tube remained constant at 0.57 g, so the mass fraction of (Fe,Ni) slightly increased during the process, serving as an excellent internal standard for quantification. (b) An Avrami plot yields the rate constant k and the time component n as shown in the plot.

The *Rietveld* least-square fittings were performed with the aid of the computer program GSAS;[24,25] structure models for least-square fittings were obtained from the Inorganic Crystal Structure Database [numbers 9826 for leucite ($KAlSi_2O_6$), 2930 for analcime ($NaAlSi_2O_6 \cdot H_2O$), and 103559 for the stainless steel mesh sample tube (Fe,Ni)].

The kinetics was then modeled by the *Avrami* equation[26]

$$\ln \ln[1/(1-y)] = n \ln k + n \ln t. \quad (5)$$

From Eq. (5), the rate constants k and the reaction-mechanism dependent time exponent n were extracted by plotting $\ln \ln[1/(1-y)]$ versus $\ln t$.

The activation energy of the reaction can be calculated by plotting $\ln k$ versus $1000/T$ through the *Arrhenius* equation[27]

$$k = Ae^{-E_a/RT}, \quad (6)$$

where A is pre-exponential factor, E_a is the activation energy of the reaction ($J\ mol^{-1}$), R is the gas constant ($8.3145\ J\ K^{-1}\ mol^{-1}$), and T is temperature in Kelvin scale (K).

The *in situ* diffraction patterns are shown in Fig. 3. It is clearly seen that the analcime diffraction peaks increase with time at the expense of those from leucite; the stainless steel peaks from the mesh tube remain constant, serving as an excellent internal standard. The zero-scattering Ti–Zr alloy sample compartment has no diffraction peaks, giving an excellent flat background. No other phase was observed as reaction intermediate or byproduct. This clearly indicates the progressive transformation from leucite directly to analcime.

The transformation is more clearly seen in the mass fraction evolution plot [Fig. 4(a)], which reveals that ca. 50 wt % leucite was transformed to analcime in ca. 12 h reaction time. The slight increase of mass fraction of stainless steel from ca. 31 wt % to ca. 38 wt % is due to the slight loss of small leucite/analcime particles from the mesh tube. The mass of stainless steel mesh tube was constant before and after the experiment (0.57 g) but the mass of sample decreased from 1.25 to 0.92 g.

The Avrami plot [Fig. 4(b)] gives rate constant $k = 1.93 \pm 0.14 \times 10^{-5}\ s^{-1}$ and the time exponent $n = 2.04 \pm 0.01$. The reaction condition used in this study was identical to our previous *in situ* neutron diffraction study except the reaction temperature,[18] and the same nucleation

and growth mechanism prevails in both temperatures as indicated by the close value of n (2.09 ± 0.01 at 230 °C), we can therefore calculate the activation energy E_a of the transformation from Eq. (6), and it is 82.3 ± 1.1 kJ mol^{-1}.

Assuming that reaction mechanism does not change over a wide range of temperature from room temperature to 300 °C, the reaction rate in nature can be estimated by extrapolating based on Eqs. (5) and (6). In nature, the transformation may occur during cooling of the magma, under which condition the temperature can be as high as a few hundreds of Celsius, or after the host rock has solidified, under which condition the temperature can be as low as room temperature.[21] Also considering the proportional relationship between specific surface area and the reaction rate for hydrothermal mineral transformations,[3,17] the extrapolations estimate that in the presence of salt water (ca. 0.6M Na^+) it takes around 7600 years at 25 °C (after solidification of host rock) or only 8 h at 300 °C (cooling from magma) to completely transform a 0.5 mm (typical size) leucite crystal to analcime. This estimation suggests that if analcime is secondary origin, it is most likely transformed from leucite under hydrothermal conditions during the cooling of the magma because partially transformed leucite is very rare in nature.

V. CONCLUSIONS

We have developed a large volume cell for *in situ* neutron diffraction studies of hydrothermal crystallizations and successfully commissioned on the high intensity powder diffractometer in ANSTO. The cell can operate at temperatures up to ca. 300 °C and pressures up to ca. 90 bars, and has the flexibility to accommodate more hostile conditions by simply changing commercial standard components. The capability of the cell was demonstrated by an *in situ* kinetic study of the hydrothermal phase transformations from leucite ($KAlSi_2O_4$) to analcime ($NaAlSi_2O_6 \cdot H_2O$). The extrapolations from the kinetic results give reasonable estimation of the reaction rate in nature and suggest that the secondary analcime is mostly formed during cooling of the magma.

ACKNOWLEDGMENTS

Thanks are due to Mr. Jason Peak (Chemical Engineering Workshop at the University of Adelaide) for building up the cell and many insightful discussions and an anonymous reviewer for critical comments. This work is financially supported by the Australian Research Council (Grant No. ARC DP1095069) and the Australian Institute of Nuclear Science and Engineering (AINSE).

[1] J. Brugger, A. Pring, F. Reith, C. Ryan, B. Etschmann, W. Liu, B. O'Neill, and Y. Ngothai, Radiat. Phys. Chem. **79**, 151 (2010).
[2] A. Putnis, Rev. Mineral. Geochem. **70**, 87 (2009).
[3] F. Xia, J. Brugger, G. Chen, Y. Ngothai, B. O'Neill, A. Putnis, and A. Pring, Geochim. Cosmochim. Acta **73**, 1945 (2009).
[4] S. Venkatachalam, *Hydrometallurgy* (Narosa, New Delhi, 1998).
[5] J. Zhao, F. Xia, A. Pring, J. Brugger, P. V. Grundler, and G. Chen, Minerals Eng. **23**, 451 (2010).
[6] E. Polak, J. Munn, P. Barnes, S. E. Tarling, and C. Ritter, J. Appl. Crystallogr. **23**, 258 (1990).
[7] J. S. O. Evans, R. J. Francis, D. O'Hare, S. J. Price, S. M. Clark, J. Flaherty, J. Gordon, A. Nield, and C. C. Tang, Rev. Sci. Instrum. **66**, 2442 (1995).
[8] R. J. Francis, S. O'Brien, A. M. Fogg, P. S. Halasyamani, D. O'Hare, T. Loiseau, and G. Ferey, J. Am. Chem. Soc. **121**, 1002 (1999).
[9] P. Norby, C. Cahill, C. Koleda, and J. B. Parise, J. Appl. Crystallogr. **31**, 481 (1998).
[10] P. Norby, J. Am. Chem. Soc. **119**, 5215 (1997).
[11] R. I. Walton, R. J. Francis, P. S. Halasyamani, D. O'Hare, R. I. Smith, R. Done, and R. J. Humphreys, Rev. Sci. Instrum. **70**, 3391 (1999).
[12] G. R. Williams, A. J. Norquist, and D. O'Hare, Chem. Mater. **18**, 3801 (2006).
[13] B. O'Neill, C. Tenailleau, Y. Ngothai, A. Studer, J. Brugger, and A. Pring, Physica B **385-386**, 942 (2006).
[14] N. A. S. Webster, I. C. Madsen, M. J. Loan, N. V. Y. Scarlett, and K. S. Wallwork, Rev. Sci. Instrum. **80**, 084102 (2009).
[15] W. D. Carlson, Am. Mineral. **87**, 185 (2002).
[16] F. Xia, J. Zhou, J. Brugger, Y. Ngothai, B. O'Neill, G. Chen, and A. Pring, Chem. Mater. **20**, 2809 (2008).
[17] J. Zhao, J. Brugger, P. V. Grundler, F. Xia, G. Chen, and A. Pring, Am. Mineral. **94**, 1541 (2009).
[18] F. Xia, B. O'Neill, Y. Ngothai, J. Peak, C. Tenailleau, B. Etschmann, G. Qian, J. Brugger, A. Studer, S. Olsen, and A. Pring, J. Appl. Crystallogr. **43**, 511 (2010).
[19] K. Byrappa and M. Yoshimura, *Handbook of Hydrothermal Technology: A Technology for Crystal Growth and Materials Processing* (Noyes Publications/William Andrew Publishing, LLC, Norwich, 2001), p. 870.
[20] A. J. Studer, M. E. Hagen, and T. J. Noakes, Physica B **385-386**, 1013 (2006).
[21] H. R. Karlsson and R. N. Clayton, Am. Mineral. **76**, 189 (1991).
[22] F. Xia, J. Brugger, Y. Ngothai, B. O'Neill, G. Chen, and A. Pring, Cryst. Growth Des. **9**, 4902 (2009).
[23] H. M. Rietveld, J. Appl. Crystallogr. **2**, 65 (1969).
[24] A. C. Larson and R. B. Von Dreele, Los Alamos National Laboratory Report No. LAUR 86-748, 2004.
[25] B. H. Toby, J. Appl. Crystallogr. **34**, 210 (2001).
[26] B. Etschmann, A. Pring, A. Putnis, B. A. Grguric, and A. Studer, Am. Mineral. **89**, 39 (2004).
[27] A. C. Lasaga, J. Geophys. Res. **89**, 4009 (1984).